ACS OMEGA

http://pubs.acs.org/journal/acsodf

Article

Effect of Stoichiometry and Ordering on the Microstructure of Titanium Monoxide TiO_y

Svetlana V. Rempel,* Andrey A. Rempel, and Albina A. Valeeva

Cite This: *ACS Omega* 2020, 5, 22513−22519

Read Online

ACCESS | Metrics & More | Article Recommendations

ABSTRACT: The structure of titanium monoxide TiO_y with different stoichiometries and long-range order degrees was studied by using X-ray diffraction, electron backscatter diffraction, Raman spectroscopy, and electron microscopy methods. It was established that the composition of the phases formed in annealed TiO_y depends on the titanium monoxide stoichiometry. A new phase precipitation mechanism is proposed. The migration of vacancies in dislocations and their accumulation on grain boundaries play an important role in the formation of new phases. The stoichiometry of quenched titanium monoxide (TiO_y) was found to affect the intensity of the peak associated with the vibrational mode of the Ti−O bond in Raman spectra.

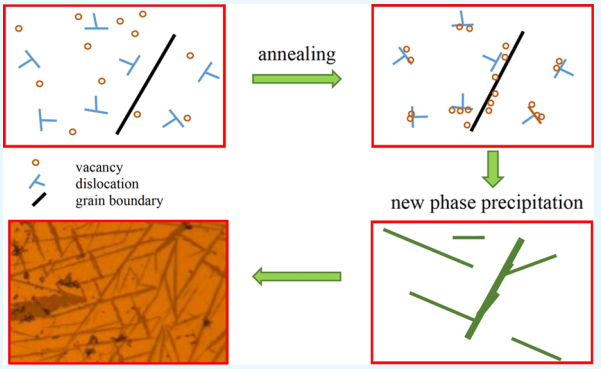

INTRODUCTION

The Ti−O system attracts much attention of researchers from both fundamental and applied viewpoints.[1−5] Titanium monoxide (TiO_y) is a special compound in this system. It possesses a wide homogeneity region ($0.8 > y > 1.3$) and contains up to 16 at. % structural vacancies in both titanium and oxygen sublattices simultaneously.[6−12] Such considerable amount of vacancies results in significant differences in the properties of substoichiometric, stoichiometric, and superstoichiometric TiO_y in both ordered and disordered states.[13−18] In addition, a size effect was detected in the properties of nonstoichiometric titanium monoxide nanocrystals.[19−23] Earlier in ref 24, mechanical and annealing twins, longitudinal and transverse cleavage steps due to intermittent motion of twin boundaries had been found in nonstoichiometric titanium monoxide. When the stoichiometry changed, the curvature of cleavage edges because of the effect of defects (vacancies) and elastic stress inhomogeneity was observed. Thus, until now, the studies of the ordered phases of titanium monoxide TiO_y had been limited to crystal symmetry and defect determination. The identification of precipitated phases in the matrix with a cubic structure had not been carried out, and the effects of the defects on the structure and mechanism of the vacancy migration had not been studied. The purpose of this work was to analyze in detail the precipitated phases, to identify them, and to search for the possible mechanisms of precipitation of additional phases in the matrix with a cubic structure, as well as the mechanisms of vacancy migration in nonstoichiometric titanium monoxide which have vacancies in two sublattices simultaneously.

RESULTS AND DISCUSSION

The presence of a large number of structural vacancies in the titanium and oxygen sublattices of nonstoichiometric titanium monoxide TiO_y leads to a variation in the quantity of Ti−O bonds. The length of some bonds may also change because of the electronic density distortions induced by defects. Such changes should result in different intensities and positions of vibrational bands of Ti−O bonds in case of substoichiometric and superstoichiometric compositions, as well as in comparison with TiO_2. Moreover, when the temperature rises and diffusion processes are activated, the difference in stoichiometry should lead to different phase compositions.

In the crystal lattice of stoichiometric TiO_y, each Ti atom is surrounded by six O atoms, whereas in nonstoichiometric TiO_y, the probability of such environment is low, and the most likely environment is five O atoms and one O vacancy. The possible configurations of clusters with structural vacancies in transition-metal monoxides are considered in ref 10. In order to designate vacancies in both TiO_y sublattices, the composition is written as $Ti_x\blacksquare_{1-x}O_z\square_{1-z}$, where x and z are the fractions of atomic positions in titanium and oxygen sublattices, respectively; ■ and □ are the structural vacancies in these sublattices; and $y = z/x$. To estimate the number of

Received: June 29, 2020
Accepted: August 7, 2020
Published: August 24, 2020

https://dx.doi.org/10.1021/acsomega.0c03122
ACS Omega 2020, 5, 22513−22519

Ti−O bonds per one mole of substance for the initial TiO_y powders, it is possible to use the experimental dependence[25] of the fraction of atomic positions in titanium and oxygen sublattices on y in TiO_y. The estimated number of Ti−O bonds per one mole of substance is 5.35 for superstoichiometric TiO_y and 5.27 for substoichiometric TiO_y. Such difference in the number of bonds should give different contributions to the Raman spectra for substoichiometric and superstoichiometric TiO_y (the stoichiometric composition is intermediate, and the difference with the other compositions will be less essential). The Raman spectra of nonstoichiometric quenched TiO_y nanopowders are presented in Figure 1.

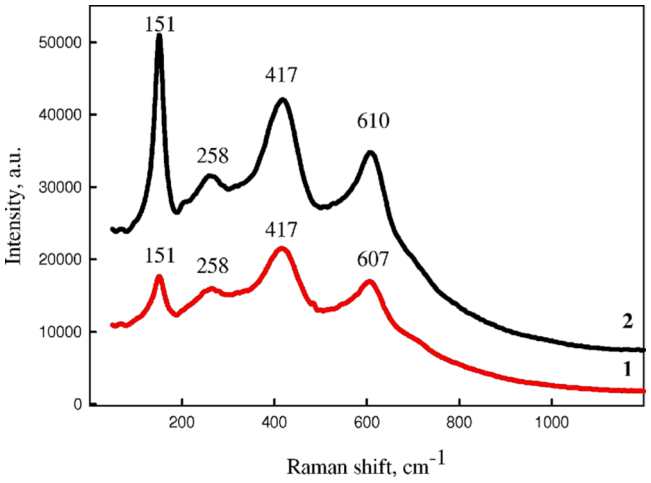

Figure 1. Raman spectra of quenched $TiO_{0.92}$ (1) and $TiO_{1.23}$ (2) nanopowders after 480 min of milling.

The frequency region below 600 cm^{-1} provides information on the structure of the coordination sphere and the character of metal−ligand bonding. The main bands of the obtained spectra coincide with the bands detected by Nguyen and He[19] in the Raman spectra of the synthesized, milled, and annealed TiO_y powders.

The spectra of quenched substoichiometric $TiO_{0.92}$ and superstoichiometric $TiO_{1.23}$ feature peaks at 151, 258, 417, and 607 (610) cm^{-1}. For substoichiometric $TiO_{0.92}$, the intensity of the peak with the maximum in the region of 151 cm^{-1} is close to that of the peak at 607 cm^{-1}. For superstoichiometric $TiO_{1.23}$, the peak at 151 cm^{-1} has the maximal intensity. In ref 19, instead of the band at 151 cm^{-1}, a band at 144 cm^{-1} is observed, which has the smallest intensity among all peaks. In different studies,[26,27] the peak at 144 cm^{-1} of the vibrational mode (E_g) in the spectrum of TiO_2 (anatase) is related to disordering, anharmonicity, oxygen deficiency, or titanium valence variation. The dependence of the position and intensity of peaks on the ratio of O/Ti content was observed in ref 28. In the spectra of the examined TiO_y powders, the relative intensity of the peak at 151 cm^{-1} that can be attributed to the vibrational mode (E_g) increases when the relative proportion of Ti in TiO_y lowers. The growth of the number of Ti−O bonds corresponds to the enhancement of the relative intensity of the peak at 151 cm^{-1} in the Raman spectrum. All the above-stated facts allow us to hypothesize that the shift and the value of the relative intensity of the band in the region of 144−151 cm^{-1} are indicative of the variation in the relative content of vacancies and bond length in the Ti−O system. As isopropyl alcohol was used as the grinding liquid during milling, the adsorbed carbon is usually present on the surface of nanoparticles.

Owing to a large number of vacancies, the processes of ordering during annealing and quenching in substoichiometric and superstoichiometric TiO_y take place with the formation of new phases; thus, a relationship between the microstructure and stoichiometry was observed in ref 24. To identify the new phases and clarify their formation mechanism, the microstructure and phase composition were studied with scanning electron microscopy (SEM) and energy-dispersive X-ray (EDX)methods. Figure 2 displays the micrographs of the surface of annealed substoichiometric $TiO_{0.92}$.

According to the results of X-ray phase analysis, titanium monoxide $TiO_{0.92}$ contains 20% of disordered cubic phase TiO_y (sp. gr. $Fm\bar{3}m$), 75% of ordered monoclinic phase Ti_5O_5 (sp.gr. $C2/m$), and about 5% of Ti_2O phase (sp.gr. $P\bar{3}m1$). Coarse grains are observed in the sample. On the grain boundaries and also inside them, an additional phase is precipitated, which, judging by the superposition of the two spectra, is enriched with titanium in comparison with the basic phase. The relative content of oxygen and titanium in the precipitated phase could not be determined because the precipitation areas were smaller than the minimal region of the EDX analysis. According to the superposition of the EDX spectra, the areas with smaller contrast are rich in titanium, which is also confirmed by a lighter picture on the backscattered electron (BSE) image. The directions of the ordered monoclinic phase growth are specified by the matrix cubic phase.

Figure 3 demonstrates the micrographs of the annealed titanium monoxide $TiO_{0.99}$ thin section surface. The microstructure is homogeneous, and grain boundaries are observed.

No precipitation of additional phases inside grains or on grain boundaries was found in the ordered titanium monoxide $TiO_{0.99}$. According to the X-ray phase analysis, titanium monoxide $TiO_{0.99}$ contains only the ordered monoclinic Ti_5O_5 (sp.gr. $C2/m$) and disordered cubic TiO_y (sp. gr. $Fm\bar{3}m$) phases. The small low-contrast inclusions are likely to be the grains of the monoclinic phase.

Figure 4 presents the micrographs of the annealed titanium monoxide $TiO_{1.26}$ thin section surface.

The precipitation of additional phases in the annealed titanium monoxide $TiO_{1.26}$ is clearly seen. These phases contrast with the basic matrix and with each other on the BSE image. The precipitation of secondary phases has a form of crossing bands. Most of such bands have ragged edges, but there are bands with smooth soft edges as well. The difference in the band patterns allows us to hypothesize the precipitation of at least two different secondary phases. Although the local character of the EDX method does not enable finding the exact proportions of elements in the phases, it can be concluded from the darker color and spectra superposition that they are oxygen-enriched in comparison with the basic phase. The presence of the Ti_2O_3 phase can be determined by using the EDX analysis of oxygen stoichiometry. According to the results of X-ray phase analysis, besides the reflections corresponding to the basic cubic phase, additional reflections of the ordered trigonal phase Ti_2O_3 (sp. gr. $R\bar{3}c$) with corundum structure are present. The content of the second oxygen-rich phase is too small to be determined with the X-ray phase analysis method. New phases are formed on the boundaries of different types and their interfaces, on dislocation edges, and in the regions

https://dx.doi.org/10.1021/acsomega.0c03122
ACS Omega 2020, 5, 22513−22519

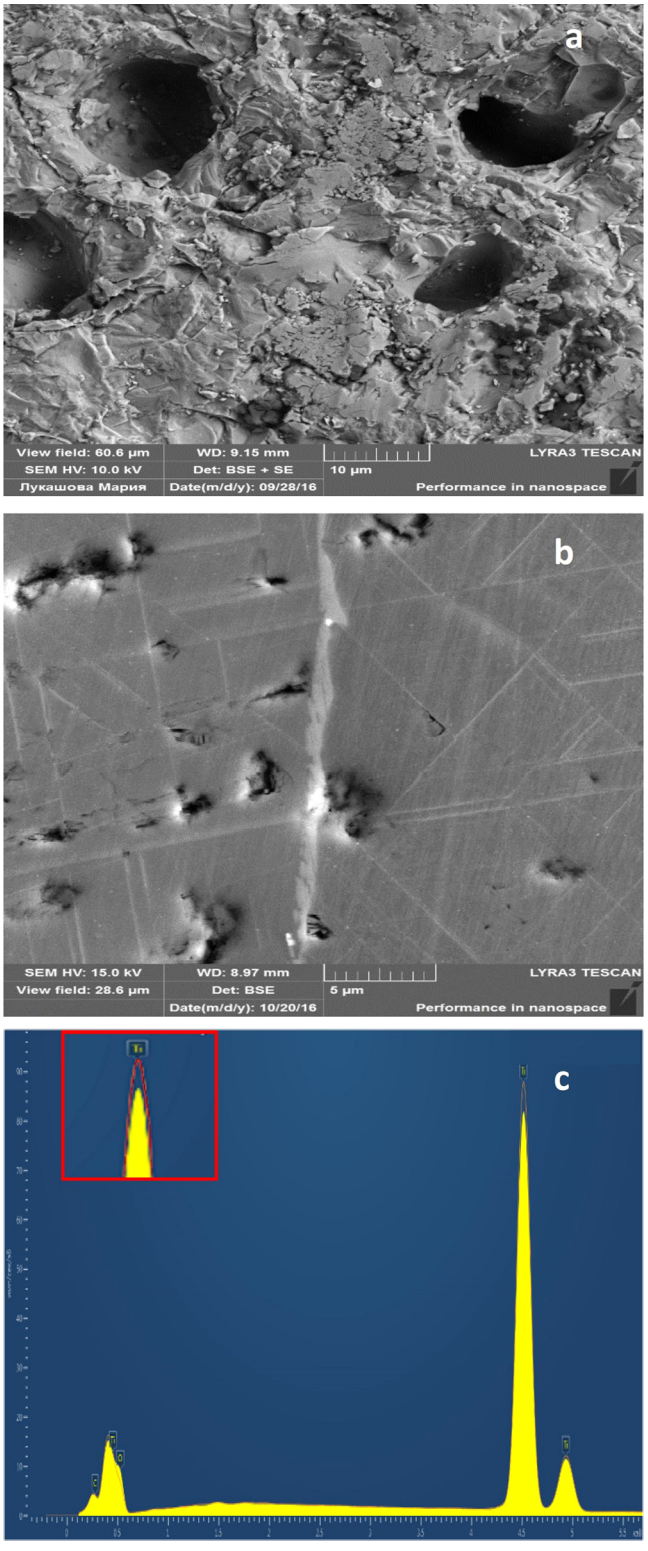

Figure 2. Microstructure of the annealed titanium monoxide $TiO_{0.92}$ thin section surface and the EDX result in the basic matrix and in the region of inclusions: (a) macroscopic pores; (b) precipitation of titanium-enriched phase on the grain boundaries and in the regions where dislocations intersect the surface; (c) intensity of O and Ti lines obtained with the EDX method in the basic matrix (yellow) and in the region of inclusions.

where the dislocations intersect the surface or interact with point defects.

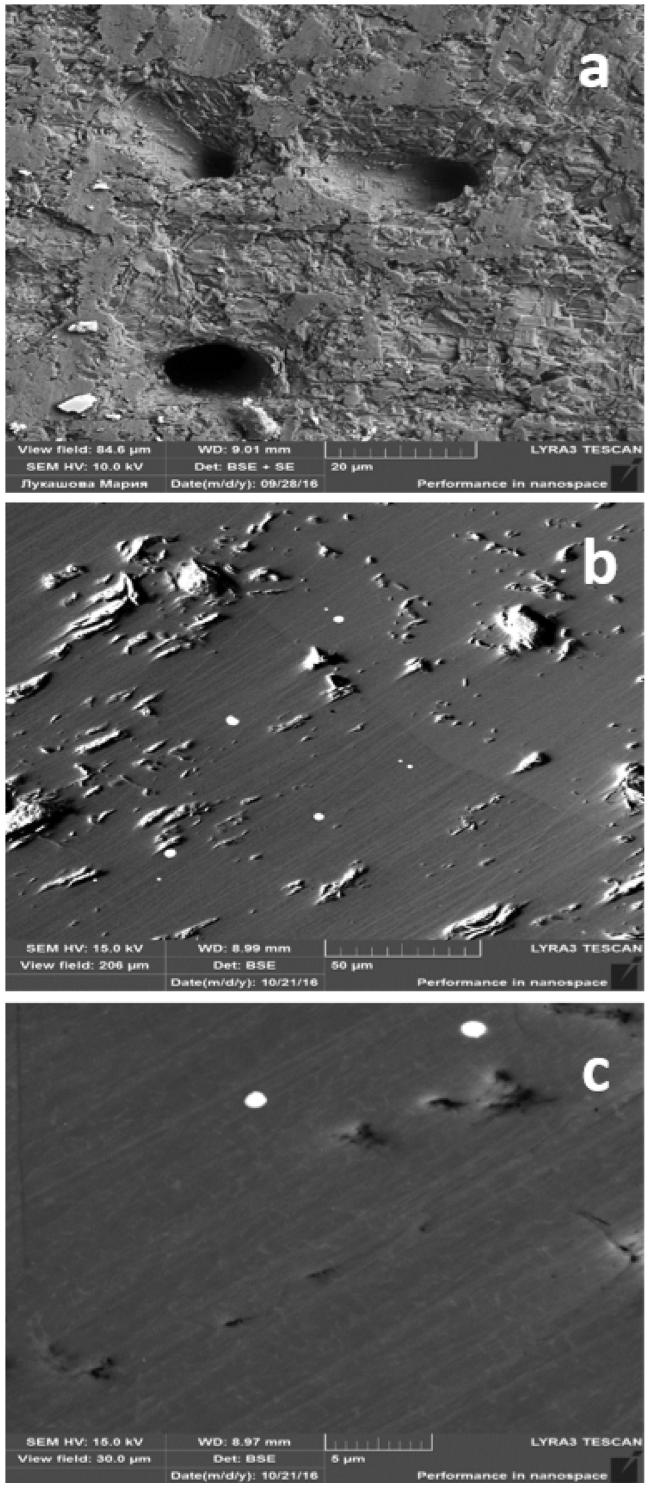

Figure 3. Microstructure of the annealed titanium monoxide $TiO_{0.99}$ thin section surface: (a) macroscopic pores; (b) grain boundary with different crystal orientations; (c) inclusions of the monoclinic phase.

The phase composition of superstoichiometric annealed titanium monoxide $TiO_{1.26}$ was studied by using the electron backscatter diffraction (EBSD) method. The matrix was examined primarily. Figure 5 demonstrates the BSE diffraction patterns obtained when the basic matrix was scanned, indexing of Kikuchi bands, and the unit cell position. The research results reveal that the matrix contains the cubic phase (sp. gr. $Fm\bar{3}m$) TiO_y.

https://dx.doi.org/10.1021/acsomega.0c03122
ACS Omega 2020, 5, 22513−22519

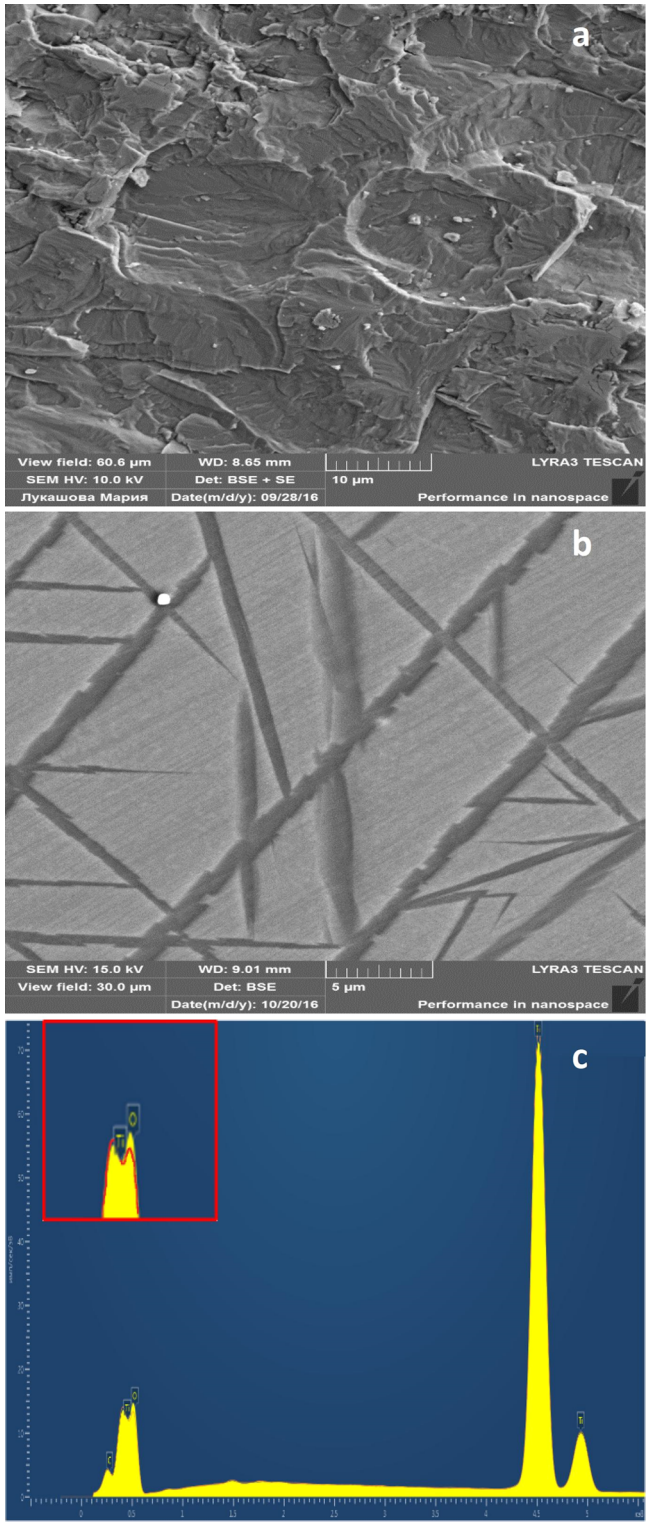

Figure 4. Microstructure of the annealed titanium monoxide $TiO_{1.26}$ thin section surface and the EDX result in the basic matrix and in the region of inclusions: (a) surface of superstoichiometric TiO_y; (b) precipitation of oxygen-rich phases; (c) intensity of O and Ti lines obtained with the EDX method in the basic matrix and in the region of inclusions (yellow).

The phases precipitated in the form of darker bands and needles were studied. Figures 5 and 6 present the Kikuchi patterns for additional phases.

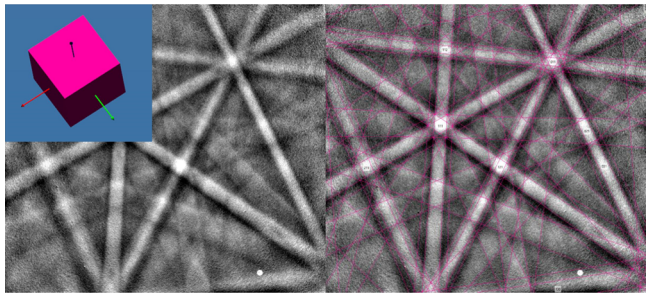

Figure 5. BSE diffraction pattern (Kikuchi pattern) of the basic phase (matrix). Indexing of Kikuchi bands for the matrix, and the unit cell position of the cubic structure to obtain Kossel cones. The average angular deflection (AAD) is 0.17°.

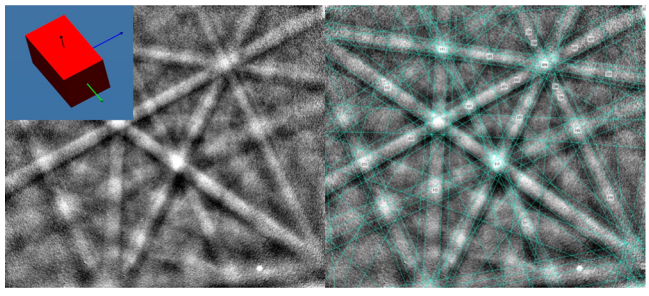

Figure 6. BSE diffraction pattern (Kikuchi pattern) of the precipitated phases. Indexing of Kikuchi bands for additional phases, and the unit cell position for obtaining Kossel cones. The AAD is 0.24°.

According to EBSD data, the precipitated phases are oxygen-enriched and have an orthorhombic structure of $Ti_{4.5}O_5$ (sp. gr. *Immm*). The AAD of the observed Kikuchi bands is 0.25–0.35° in all the cases, a coincidence for 11 bands, which indicates a good agreement of the proposed structure. The data of quantum chemical calculations show that the $Ti_{4.5}O_5$ phase (sp. gr. *Immm*) is formed only during the transition from a crystalline phase to a nanostate.[29−31] This phase was first prepared during the annealing of nonstoichiometric TiO_y nanocrystals and TiO_y/HAP nanocomposites; the formation of the $Ti_{4.5}O_5$ phase occurs during the annealing of the titanium oxide nanocrystals of superstoichiometric composition only.[32−34]

It was found by using the X-ray phase analysis that besides the reflections corresponding to the basic cubic phase, there are additional reflections of only one ordered trigonal phase Ti_2O_3 (sp. gr. $R\bar{3}c$). The differences in the band pattern allow us to hypothesize the precipitation of at least two different secondary phases. The presence of the Ti_2O_3 phase was determined by EDX analysis of oxygen stoichiometry. At the same time, the EBSD method revealed the presence of only the $Ti_{4.5}O_5$ phase. Thus, the matrix contains the cubic phase (sp. gr. $Fm\bar{3}m$) TiO_y, and the dark precipitated phases are Ti_2O_3 and $Ti_{4.5}O_5$. The analysis of the micrographs obtained with the use of optical microscopy shows that the phases are distributed nonuniformly. The content of the Ti_2O_3 phase is sufficient for it to be found with the X-ray phase analysis method. The content of the second phase $Ti_{4.5}O_5$ is insufficient for it to be found by using X-ray phase analysis and EDX methods; it is distributed mostly on the surface, which allows its identification with the EBSD method.

According to the performed investigations and analysis of the crystal structure by using the abovementioned methods, a

https://dx.doi.org/10.1021/acsomega.0c03122
ACS Omega 2020, 5, 22513−22519

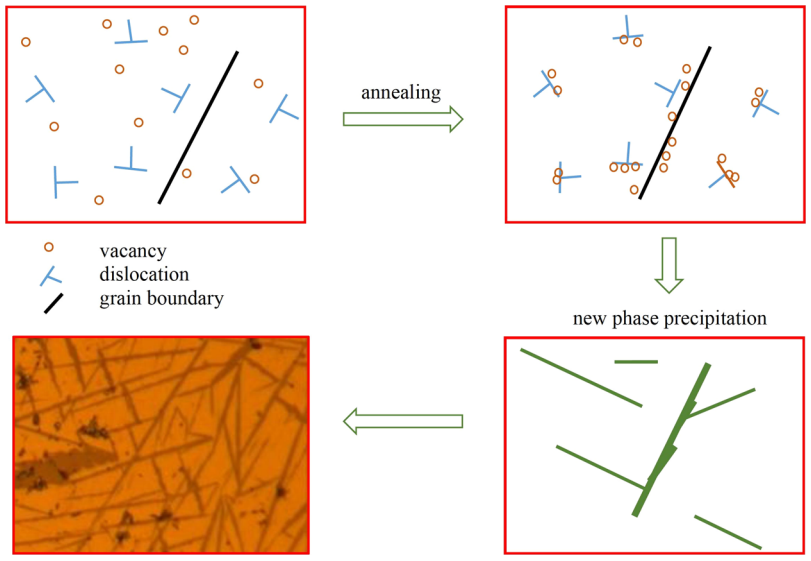

Figure 7. Scheme of the additional phase precipitation mechanism of nonstoichiometric TiO_y.

phase precipitation mechanism during heat treatment in nonstoichiometric TiO_y, which have up to 16 at.% structural vacancies in both titanium and oxygen sublattices simultaneously, was proposed (Figure 7).

The character of precipitation of additional phases in all cases indicates the migration of dislocations during heat treatment. The diffusion of vacancies in dislocations is faster than usual diffusion. Vacancies accumulate and collapse forming open and closed pores which are observed on the surface after annealing. The accumulation of vacancies on the grain boundaries and linear defects of the crystal structure makes these bands enriched with the atoms of the second element. When the concentration of vacancies exceeds the permissible concentration in one of the sublattices, a phase transition takes place, giving rise to a new phase. The composition of the formed phase depends on the initial distribution of vacancies in the sublattices, that is, on the initial stoichiometry. Thus, in substoichiometric titanium monoxide, a titanium-rich phase is precipitated, and in superstoichiometric oxide—an oxygen-rich phase. The fact that the directions of growth of new phases are specified by the matrix cubic phase confirms the assumption that the diffusion of vacancies in dislocations is the main mechanism which precedes the phase transitions with the formation of new phases: Ti_2O, Ti_2O_3, and an additional oxygen-rich phase.

CONCLUSIONS

In the present work, the formation of new phases in TiO_y with different stoichiometries is studied in detail. The stoichiometry of titanium monoxide (TiO_y) affects the intensity of the peak associated with the vibrational mode of Ti−O bond in Raman spectra. The phase precipitation mechanism of nonstoichiometric TiO_y which contains up to 16 at. % structural vacancies in both titanium and oxygen sublattices is simultaneously proposed. The composition of the formed phase depends on the initial distribution of vacancies in the sublattices, that is, on the initial stoichiometry. The migration of vacancies in dislocations and their accumulation on grain boundaries play an important role in the formation of new phases.

EXPERIMENTAL SECTION

Microcrystals of titanium monoxide TiO_y with different oxygen contents (y = 0.92, 0.99, 1.26), with the average size of about 25 μm, have been synthesized by using the solid-phase sintering method from a mixture of metallic Ti and TiO_2 powders under a 10^{-3} Pa vacuum at a temperature of 1773 K. According to the X-ray phase analysis data, the synthesized samples of titanium monoxide contained two phases—disordered cubic phase (sp. gr. $Fm\bar{3}m$) and ordered monoclinic phase (sp. gr. $C2/m$). For the samples to reach the disordered state, they were annealed in a vacuum for 3 h at a temperature of 1373 K, which is slightly higher than the equilibrium temperature of transition from the disordered state to the ordered one. After this, the quartz ampules with the samples were quenched into water, and the quenching rate was about 200 K/s. For the samples to reach the ordered state, they were annealed in a vacuum (10^{-3} Pa) at 1330 K for 3 h, and then the quartz ampules with the sample were slowly cooled to 300 K at a rate of 10 K/h. The degree of inhomogeneity of titanium monoxide was determined by using the technique for diffraction reflection broadening.[35] Estimates show that the examined samples are homogeneous, and the homogeneity degree is ∼0.97, that is, close to 1.0.

Nanocrystalline powders of titanium monoxide were produced with high-energy milling of microcrystals of TiO_y in a Retsch PM 200 planetary ball mill. Zirconium dioxide (ZrO_2) stabilized with yttrium oxide (Y_2O_3) was the material of milling balls and pots. The mass ratio between the milling balls and powders was 10:1. Isopropyl alcohol was used as the grinding liquid; the rotation velocity of the backing plate of milling pots was 500 rpm; and the duration of milling was 15−480 min. Owing to the fragmentation of titanium monoxides, nanoparticles of 30 ± 10 nm in size were obtained. The method for the production of nanoparticles with high-energy milling, full-profile description of X-ray diffraction spectra, and determination of coherent scattering regions are reported in ref 36.

The X-ray phase analysis of all powders was performed in Cu$K\alpha_{1,2}$ radiation on a Shimadzu XRD-7000 diffractometer in Bragg−Brentano geometry in a stepwise scanning mode with $\Delta(2\theta)$ = 0.02° in the 2θ angle interval from 10 to 120°. To

https://dx.doi.org/10.1021/acsomega.0c03122
ACS Omega 2020, 5, 22513−22519

identify the phases, the powder diffraction database ICDD, USA, Release 2016, was used. The phases were analyzed with the use of the Powder Cell 2.4 program.

The Raman spectra were obtained in the interval 50−4000 cm^{-1} at room temperature on a RENISHAW-1000 spectrometer (λ = 532 nm, P = 25 mW). Nanopowders of substoichiometric and superstoichiometric TiO_y, milled for 480 min in the presence of grinding liquid (isopropyl alcohol), were used for the investigation.

The SEM and EBSD studies were carried out on a LYRA 3 GMH (TESCAN) scanning electron microscope with a Schottky cathode and an ion column, an X-Max 80 AZtec Automated (Oxford Instrument) system for energy-dispersive spectroscopy, and a Symmetry (Oxford Instruments) system to analyze EBSD patterns.

A BSE detector was used for imaging as the BSE signal is sensitive to compositional contrast. After the objects were visualized, the elemental composition of the matrix and the object was found by EDX analysis. Each phase was analyzed in five randomly chosen points, and the average composition of grains was determined. The surface of the annealed TiO_y samples was prepared on a BUEHLER metallographic complex. Diamond emulsions with particle size of 30, 6, and 1 μm were sequentially used for polishing. The samples were polished to purity level 12, that is, until mirror-smooth finish of the treated surface appeared.

To avoid charge accumulation on the surface of the sample during electron microscopy imaging, a thin (<15 nm) carbon layer was sprayed on the surface of the samples. The carbon conducting layer was sprayed by using a Q150R E (Quorum Technologies) sputtering apparatus.

In order to obtain reliable EBSD data, particularly careful sample preparation is required as even a relatively small roughness or an oxide film on the surface may give inaccurate results.[37] The sample was polished on a LINDA SEMPrep2 (Technoorg Linda, Hungary) ion polishing apparatus. The argon ion beam energy for polishing was 5.5 keV; polishing was performed for 24 min; and the angle between the argon ion beam and the sample surface was 5°. The sample was rotated during polishing.

AUTHOR INFORMATION

Corresponding Author

Svetlana V. Rempel − *Institute of Solid State Chemistry, Ural Branch of the Russian Academy of Sciences, 620990 Ekaterinburg, Russia; Ural Federal University, 620002 Ekaterinburg, Russia;* orcid.org/0000-0002-8747-6719; Email: svetlana_rempel@ihim.uran.ru; Fax: +7 343 374 4495

Authors

Andrey A. Rempel − *Institute of Metallurgy of the Ural Branch of the Russian Academy of Sciences, 620016 Ekaterinburg, Russia; Ural Federal University, 620002 Ekaterinburg, Russia*

Albina A. Valeeva − *Institute of Solid State Chemistry, Ural Branch of the Russian Academy of Sciences, 620990 Ekaterinburg, Russia; Ural Federal University, 620002 Ekaterinburg, Russia;* orcid.org/0000-0003-1656-732X

Complete contact information is available at: https://pubs.acs.org/10.1021/acsomega.0c03122

Notes

The authors declare no competing financial interest.

ACKNOWLEDGMENTS

The authors are grateful to M. V. Lukashova (Demonstration laboratory TESCAN, St. Petersburg) for her assistance in carrying out the research. The reported study was funded by RFBR according to the research project no. 19-03-00051a.

REFERENCES

(1) Chen, X.; Mao, S. S. Titanium Dioxide Nanomaterials: Synthesis, Properties, Modifications, and Applications. *Chem. Rev.* **2007**, *107*, 2891−2959.

(2) Rempel, A. A.; Valeeva, A. A. Nanostructural titanium dioxide for medical chemistry. *Russ. Chem. Bull.* **2019**, *68*, 2163−2171.

(3) Valeeva, A. A.; Kozlova, E. A.; Vokhmintsev, A. S.; Kamalov, R. V.; Dorosheva, I. B.; Saraev, A. A.; Weinstein, I. A.; Rempel, A. A. Nonstoichiometric titanium dioxide nanotubes with enhanced catalytical activity under visible light. *Sci. Rep.* **2018**, *8*, 9607.

(4) Valeeva, A. A.; Dorosheva, I. B.; Kozlova, E. A.; Kamalov, R. V.; Vokhmintsev, A. S.; Selishchev, D. S.; Saraev, A. A.; Gerasimov, E. Y.; Weinstein, I. A.; Rempel, A. A. Influence of calcination on photocatalytic properties of nonstoichiometric titanium dioxide nanotubes. *J. Alloys Compd.* **2019**, *796*, 293−299.

(5) Popkov, V. I.; Bachina, A. K.; Valeeva, A. A.; Lobinsky, A. A.; Gerasimov, E. Y.; Rempel, A. A. Synthesis, morphology and electrochemical properties of spherulite titania nanocrystals. *Ceram. Int.* **2020**, DOI: 10.1016/j.ceramint.2020.06.233.

(6) Andersson, S.; Collén, B.; Kuylenstierna, U.; Magnéli, A.; Magnéli, A.; Pestmalis, H.; Åsbrink, S. Phase-analysis studies on the titanium - oxygen system. *Acta Chem. Scand.* **1957**, *11*, 1641−1652.

(7) Hilti, E. Neue Phasen in System Titan-Sauerstoff. *Naturwissenschaften* **1968**, *55*, 130−131.

(8) Wahlbeck, P. G.; Gilles, P. W. Reinvestigation of the phase diagram for the system titanium-oxygen. *J. Am. Ceram. Soc.* **1966**, *49*, 180−183.

(9) Kostenko, M. G.; Valeeva, A. A.; Rempel, A. A. Octahedral clusters in various phases of nonstoichiometric titanium monoxide. *Mendeleev Commun.* **2012**, *22*, 245−247.

(10) Rempel, A. A.; Valeeva, A. A. Thermodynamics of atomic ordering in nonstoichiometric transition metal monoxides. *Mendeleev Commun.* **2010**, *20*, 101−103.

(11) Valeeva, A. A.; Rempel, A. A.; Sprengel, W.; Schaefer, H.-E. Investigation of structural vacancies in titanium monoxide by electron-positron annihilation. *Phys. Solid State* **2009**, *51*, 924−929.

(12) Valeeva, A. A.; Rempel, A. A. Cluster probabilities in ordered titanium monoxide TiOy as function of the long-range order parameters. *JETP Lett.* **2008**, *88*, 172−177.

(13) Valeeva, A. A.; Rempel, A. A.; Pfitzner, A. Elimination of vacancies in titanium monoxide under high pressure in combination with high temperature. *Monatsh. Chem.* **2015**, *146*, 1205−1209.

(14) Marinder, B. O. Ordered, defective structures of titanium monoxide, the anti-anatase structure and related structures described through an open packing on cube units (die packing). *Chem. Scr.* **1981**, *4*, 169−175.

(15) Kostenko, M. G.; Valeeva, A. A.; Rempel', A. A. Relationship between short- and lang range orders in nonstoichiometric titanium monoxide (TiO_y). *JETP Lett.* **2010**, *111*, 786−795.

(16) Watanabé, D.; Castles, J. R.; Jostsons, A.; Malin, A. S. The ordered structure of TiO. *Acta Crystallogr.* **1967**, *23*, 307−313.

(17) Rempel, A. A.; Van Renterghem, W.; Valeeva, A. A.; Verwerft, M.; Van der Berghe, S. In situ disordering of monoclinic titanium monoxide Ti_5O_5 studied by transmission electron microscope TEM. *Sci. Rep.* **2017**, *7*, 10769.

(18) Amano, S.; Bogdanovski, D.; Yamane, H.; Terauchi, M.; Dronskowski, R. ϵ-TiO, a novel stable polymorph of titanium monoxide. *Angew. Chem., Int. Ed.* **2016**, *55*, 1652−1657.

(19) Nguyen, T.-T.-N.; He, J.-L. Preparation of Titanium Monoxide Nanopowder by Low-Energy Wet Ball-Millin. *Adv. Powder Technol.* **2016**, *27*, 1868−1873.

(20) Valeeva, A. A.; Nazarova, S. Z.; Rempel, A. A. Size effect on magnetic susceptibility of titanium monoxide nanocrystals. *Phys. Status Solidi B* **2016**, *253*, 392−396.
(21) Gusev, A. I. High-energy ball milling of nonstoichiometric compounds. *Phys.-Usp.* **2020**, *63*, 342−364.
(22) Rempel, A. A.; Valeeva, A. A.; Kurlov, A. S.; Klinser, G.; Sprengel, W. Size effect in nonstoichiometric titanium monoxide and vanadium carbide nanocrystals measured by positron lifetime spectroscopy. *Mendeleev Commun.* **2019**, *29*, 486−488.
(23) Kostenko, M. G.; Valeeva, A. A. Disorder-order phase transition in nanocrystalline titanium monoxide with two-sublattice ordering of structural vacancies. *Mendeleev Commun.* **2019**, *29*, 405−407.
(24) Valeeva, A. A.; Rempel, S. V.; Schroettner, H.; Rempel, A. A. Influence of the degree of order and nonstoichiometry on microstructure and microhardness of titanium monoxide. *Inorg. Mater.* **2017**, *53*, 1174−1179.
(25) Valeeva, A. A.; Rempel, A. A.; Gusev, A. I. Ordering of Cubic Titanium Monoxide into Monoclinic Ti_5O_5. *Inorg. Mater.* **2001**, *37*, 603−612.
(26) Balaji, S.; Djaoued, Y.; Robichaud, J. Phonon Confinement Studies in Nanocrystalline Anatase-TiO_2 Thin Films by Micro Raman Spectroscopy. *J. Raman Spectrosc.* **2006**, *37*, 1416−1422.
(27) Prusakova, V.; Collini, C.; Nardi, M.; Tatti, R.; Lunelli, L.; Vanzetti, L.; Lorenzelli, L.; Baldi, G.; Chiappini, A.; Chiasera, A.; Ristic, D.; Verucchi, R.; Bortolotti, M.; Dirè, S. The Development of Sol-Gel Derived TiO_2 Thin Films and Corresponding Memristor Architectures. *RSC Adv.* **2017**, *7*, 1654−1663.
(28) Parker, J. C.; Siegel, R. W. Calibration of the Raman Spectrum to the Oxygen Stoichiometry of Nanophase TiO_2. *Appl. Phys. Lett.* **1990**, *57*, 943.
(29) Valeeva, A. A.; Kostenko, M. G.; Nazarova, S. Z.; Gerasimov, E. Y.; Rempel, A. A. New Ti_9O_{10} nanophase prepared by heat-treating nonstoichiometric milled TiO_y nanopowder. *Inorg. Mater.* **2018**, *54*, 568−574.
(30) Valeeva, A. A.; Kostenko, M. G. Stable Ti_9O_{10} nanophase grown from nonstoichiometric titanium monoxide TiO_y. *Nanosyst.: Phys., Chem., Math.* **2017**, *8*, 816−822.
(31) Kostenko, M. G.; Valeeva, A. A. Disorder-order phase transition in nanocrystalline titanium monoxide with two-sublattice ordering of structural vacancies. *Mendeleev Commun.* **2019**, *29*, 405−407.
(32) Rempel, S. V.; Valeeva, A. A.; Bogdanova, E. A.; Schroettner, H.; Sabirzyanov, N. A.; Rempel, A. A. Vacuum-made nanocomposite of low-temperature hydroxyapatite (HAp) and hard nonstoichiometric titanium monoxide (TiO_y) with enhanced mechanical properties. *Mendeleev Commun.* **2016**, *26*, 543−545.
(33) Rempel, S. V.; Eselevich, D. A.; Gerasimov, E. Y.; Valeeva, A. A. Impact of titanium monoxide stoichiometry and heat treatment on the properties of TiOy/HAp nanocomposite. *J. Alloys Compd.* **2019**, *800*, 412−418.
(34) Rempel, S. V.; Bogdanova, E. A.; Valeeva, A. A.; Schroettner, H.; Sabirzyanov, N. A.; Rempel, A. A. Microhardness and phase composition of TiOy/hydroxyapatite nanocomposites synthesized under low-temperature annealing conditions. *Inorg. Mater.* **2016**, *52*, 476−482.
(35) Rempel, A. A.; Rempel, S. V.; Gusev, A. I. Quantitative assessment of homogeneity of nonstoichiometric compounds. *Dokl. Phys. Chem.* **1999**, *369*, 321−325.
(36) Valeeva, A. A.; Schröttner, H.; Rempel, A. A. Fragmentation of disordered titanium monoxide of stoichiometric composition. *Russ. Chem. Bull.* **2014**, *63*, 2729−2732.
(37) Lukashova, M. V. Universal Sample Preparation Method for Local Phase EBSD-Analysis. Industrial laboratory. *Diagn. Mater.* **2016**, *82*, 42−46.

https://dx.doi.org/10.1021/acsomega.0c03122
ACS Omega 2020, 5, 22513−22519